Journal of the Brazilian Society of Mechanical Sciences and Engineering (2019) 41:455
https://doi.org/10.1007/s40430-019-1946-x

TECHNICAL PAPER

Structural design and stress analysis of a high-speed turbogenerator assembly supported by hydrodynamic bearings

Rodrigo T. Bento[1,2] · **André Ferrus Filho**[3] · **Marco A. Fumagalli**[3]

Received: 5 February 2019 / Accepted: 9 September 2019 / Published online: 24 September 2019

Abstract
Turbine and bushing bearing are the most critical components of high-speed machines. This paper describes the design of a high-speed turbine supported by hydrodynamic bearings. The mathematical dimensioning and the FEM analysis are presented to validate the mechanical strength of the turbine and the bushing bearing models. Fatigue life and factor of safety are also determined. The simulations show that the maximum von Mises stress values obtained are associated with the centrifugal force generated by the system rotational movement. The results variation is mainly due to the properties of the materials proposed. For the turbine, 7075-T6 aluminum alloy and SAE 4340 steel obtained satisfactory behavior under a constant operating speed of 30,000 RPM. For the hydrodynamic bearing, the TM23 bronze alloy exhibited excellent results, without fracture, and low mechanical deformation. The models exhibited a great potential employment in several applications, such as biogas systems to generate electrical energy, and educational test bench for thermodynamic and tribological simulations.

Keywords High-speed machines · Structural design · Steam turbine · Hydrodynamic bearings · FEM analysis

List of symbols

μ_d	Coefficient of dynamic friction
$A\alpha$	Turbine full-arc
C_y	Blades theoretical velocity
D_m	Mean blade diameter
F_f	Dynamic friction force
F_N	Normal force
h_e	Input enthalpy
h_s	Output enthalpy
$\dot{m}$	Mass flow
η_i	Internal efficiency
η_m	Mechanical efficiency
R	Mean radius of blades length
u	Tangential velocity
v_m	Mean velocity coefficient
$\dot{W}$	Power
Z	Number of blades
Z_{min}	Minimum number of blades
γ	Specific internal work
ε	Coefficient of laminar steam flow
ω	Angular velocity

Technical Editor: Paulo de Tarso Rocha de Mendonça, Ph.D.

✉ Rodrigo T. Bento
rodrigo.bento@ipen.br

[1] Nuclear and Energy Research Institute, IPEN–CNEN/SP, University of São Paulo, Prof. Lineu Prestes Avenue 2242, São Paulo, Brazil

[2] Universidade São Judas Tadeu, São Paulo, Brazil

[3] Faculdade de Tecnologia Termomecanica, Salvador Arena Foundation, São Bernardo do Campo, São Paulo, Brazil

1 Introduction

The utilization of thermal resources for the energy generation, transportation, and carrying out daily tasks was always considered useful for society. However, due to the concern about Brazilian energy matrix concentrated on water resources, alternative sources of energy generation are increasingly studied [1–3]. Turbogenerators are closed-circuit exothermic rotary motors that convert kinetic energy—produced by water, gas, or steam—into mechanical work in the form of torque and rotation speed of rotation [4]. This generated energy is transferred to an shaft, and it can be used efficiently for the pumps drive, compressors, turboblowers, propulsion, electric generators, among other several applications. Such efficiency is justified since this type of machine can operate at frequencies an order of magnitude above line frequency, which allows to reduce the size of the machines in the same power rating [5]. Currently, great percentage of

the world's energy is produced by the turbogenerators. The increase in high-speed machines use was due to the high energy efficiency provided by its operation—62.8%, considering a turbine entry temperature of 1703 K [6]—which is a low cost and low environmental impacts solution.

High-speed machines employed to electrical energy conversion have mechanical coupling and are supported by mechanical rotational bearings. Among the several bearings models, hydrodynamic bearings are widely used in turbomachines because of their ability to withstand high-load situations, high rotations, and good precision [7, 8]. In a simplified way, hydrodynamic bearings can be defined as a mechanical assembly formed by a shaft and a bushing, in which the shaft diameter is very close to the bushing inner diameter, in such a way that the gap between them is very small. This passive lubrication is generated from the bearing rotation upon reaching the hydrodynamic lubrication regime. Hydrodynamic term refers to the thin layer of fluid responsible for bearing loads, a phenomenon possible due to the generation of a pressure field in the oil, resulting from the movement of the rotor and the construction geometric characteristics. Hydrodynamic pressure depends on several factors such as system rotation, bearing clearance, diameter, bushing length, and applied load [9].

Knowing the conditions of the system in operation and the efforts required in its operation are important parameters to define the components sizing and the materials to be applied in study. The static and dynamic behavior analysis of the mechanical assembly requires an interaction between practice and theory by the mathematical computational methods. In this way, several researches have been developed around the performance of hydrodynamic bearings used in high-speed machines [10–12]. Since the finite element method (FEM) offers obvious modeling advantages, the implementation of simulations for the study of high-speed systems has been the subject of recent publications. The results enable to define the materials to be used, according to its mechanical properties and stresses required of project. Nguyen et al. [13] simulated the turbulent flow past a vertical axis wind turbine by the direct finite element method in a rotating ALE framework. The simulation results showed good validations against experimental data in parked and rotating conditions. Komori et al. [14] studied the dynamic characteristics of a high-speed turbine rotor supported by superconducting magnetic bearings. Rezaei [15] evaluated the dynamics and the aeroelastic effects of geometric nonlinearities in a wind turbine assembly by FEM model. The results revealed that the single-blade models are helpful in demonstrating the overall trends of turbine rotor aeroelasticity. Yao et al. [16] proposed the identification and optimization of unbalance parameters in a rotor-bearing assembly by the modal expansion technique, in order to provide more accurate predictions of system behavior.

The present paper shows in detail the structural design development of a high-speed turbogenerator assembly supported by hydrodynamic bearings, to be used in biogas systems to generate electrical energy. On the shaft, there is a de Laval steam turbine rotor that will act in generation mode. The machine must withstand the pressure conditions, caused by the injection of water vapor on the blades, and the centrifugal force generated by a rotation of 30,000 RPM applied to the system by an asynchronous motor. Mathematical control for the turbomachinery supported by hydrodynamic bearings is presented. The system is modeling as a simple concentrated mass when designing the components. The static behavior of the system is evaluated by the finite element method (MEF) under the desired conditions. This preliminary analysis is important to the future success of the control system design.

2 Mechanical design and calculation procedure

2.1 Turbine rotor-blade architectures modeling

Adopting the values present in Table 1, for the components dimensioning, is necessary to have knowledge of parameters such as mass flow, tangential velocity, centrifugal force, radial load, and maximum torque. These parameters are fundamental for the movements study of rotating components, verifying whether they support the requests that will be required. At the beginning, the maximum speed of the shaft is defined considering the squirrel cage induction generator (SCIG) acquired. For maximum power delivered from SCIG, the mechanical speed was set to 30,000 RPM. All the mechanical developments were made based on the Inventor® Autodesk software.

Specific internal work considers the system enthalpic variation, as defined by Eq. 1. This stagnation enthalpy variation can be determined by analyzing the flow between the blades using velocity triangle, in which V_1 and C_1 are the relative velocity and absolute velocity of the fluid at the turbine inlet,

Table 1 General parameters to calculate the turbine rotor-blade characteristics

Parameters	Value
Desired power (kW)	50
Rotation of the turbine rotor (RPM)	30,000
Operating pressure (MPa)	2.2
Exhaust steam pressure (MPa)	0.6
Steam temperature (K)	593
Input enthalpy (kJ kg^{-1})	3064
Output enthalpy (kJ kg^{-1})	2772

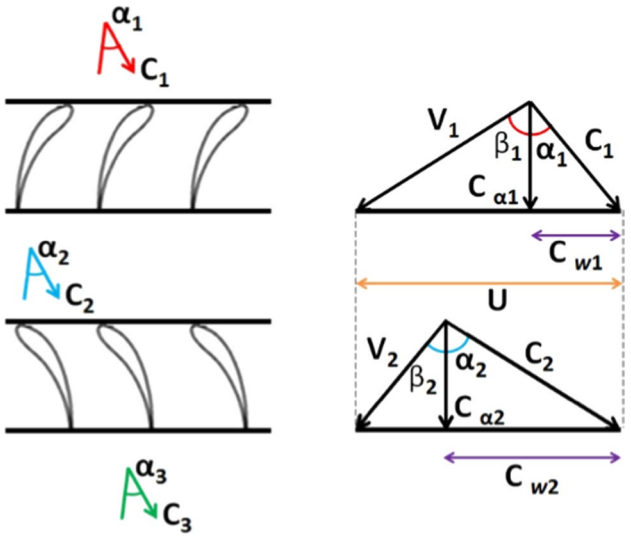

Fig. 1 Velocity triangle for the steam turbine

respectively; V_2 and C_2 are the relative velocity and absolute velocity of the fluid at the turbine outlet; C_{a1} and C_{a2} are the axial velocity of the fluid in the rotor and the stator, respectively; C_{w1} and C_{w2} are the tangential velocity of the fluid in the rotor and the stator; and U is the blade velocity. The input and output angles in the rotor are, respectively, α_1 and β_1; α_2 and β_2 are the input and output angles in the stator (Fig. 1).

$$\gamma = h_e - h_s \tag{1}$$

The fluid conditions in the transition of the stages are the same, since the absolute velocities, as the angles of entrance, are similar. The mass flow is the amount of steam consumed by the system, determined by Eq. 2. Due to the low power, the mechanical efficiencies η_i and η_m are 0.7 and 0.9, respectively, thereby obtaining a mass flow of 271.7 g s^{-1}.

$$\dot{m} = \frac{\dot{W}}{\gamma \times \eta_i \times \eta_m} \tag{2}$$

In order to operate at constant pressure, the design of a single stage rotor with partial admission was determined. Tangential velocity (Eq. 3) corresponds to the vectorial variation of position with respect to time, given by the variation in the turbine rotation. Among its main characteristics, it highlights the change of trajectory at each moment, but with its module remaining constant. Due to partial admission, the tangential velocity was estimated from the mean velocity coefficient $v_m = 0.32$—obtained by the mean value between the initial and final of the adiabatic-isentropic from Mollier diagram for water steam—and from the blades theoretical velocity (Eq. 4).

$$u = v_m \times C_y \tag{3}$$

$$C_y = \sqrt{2 \times \gamma} \tag{4}$$

Table 2 Turbine design characteristics and operating conditions

Mean turbine rotor diameter (m)	0.1556
Number of blades	20
Blade length (m)	0.04351
Blade width (m)	0.03
Full-arc turbine (m)	0.04888
Mass flow (g s^{-1})	271.7
Tangential velocity (m s^{-1})	244.6
Minimum centrifugal force (N)	1.6125×10^6
Torque (N m)	15.9155
Tangential force (N)	0.2045×10^3
Axial force (N)	0.499×10^3

The mean blade diameter (Eq. 5) was determined from the tangential velocity, as well as the number of turbine blades (Eq. 6). Cylindrical blades—with length $L = 0.04351$ m and width $b = 0.03$ m—were adopted according previous studies. The turbine full-arc value (Eq. 7) was estimated by the $\varepsilon = 0.1$. It is not advantageous to have a small number of blades, as this causes the loss of a fluid portion without doing work. Many blades are also not advantageous, since it can increase the turbine cost and can even reduce its efficiency. For safety, it is recommended to adopt a number of blades Z from 1.15 to 1.5 times greater than Z_{min}, beside a multiple value of 2 or 4. Assuming for this case 1.5 value, it was obtained a turbine with mean diameter $D_m = 0.1556$ m, and a total number of 20 blades.

$$D_m = \frac{2 \times u}{\omega} \tag{5}$$

$$Z_{min} = 12 + \left(0.7 \times \frac{R}{A_\alpha}\right) \tag{6}$$

$$A_\alpha = \pi \times D_m \times \varepsilon \tag{7}$$

The centrifugal force, torque, tangential force, and axial force values, resulting in the turbine rotor, were estimated according to the calculated dimensional parameters and are presented in Table 2.

2.2 Hydrodynamic bearing modeling

The most commonly determinant criterion for selecting a bearing is the least possible friction, defined as an actuating force contrary to the relative movement of the contact surfaces [17], or dynamic friction force (Eq. 8). Its intensity is proportional to the normal force intensity. So as to reduce the friction between the sliding bushing bearing and the rotary shaft, the use of a hydrodynamic lubrication was selected in order to replace it with a viscous friction of a lubricating fluid.

Table 3 Mathematical method for the calculation of bearing clearance (*ho*)

For shaft diameter around	Bearing clearance (*ho*)
25 to 50 mm	D/1000
50 to 100 mm	D/1500
100 to 200 mm	D/2000

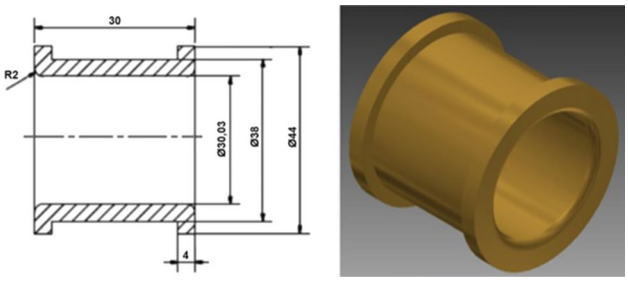

Fig. 2 Hydrodynamic bearing design with its calculated final bushing dimensions

$$F_f = \mu_d \times F_N \tag{8}$$

Hydrodynamic pressure depends on several factors, such as the system rotation, the bearing clearance, bushing diameter and length, and applied load. As the damping and stiffness of a bearing are highly sensitive to the gap (*ho*), this parameter is extremely important for the assembly dynamics control. Bearing clearance *ho* is defined by Table 3, where *D* is the shaft diameter. Considering that the shaft diameter where the bearings will be allocated is $D = 30$ mm [5], the bearing clearance value was $ho = 0.03$ mm. The other constructive measures of the bushing bearing were obtained according to DIN 1850-5 standard [18]. Bushing bearing modeling was performed by the presented methodology from the available dimensional parameters. Figure 2 shows the hydrodynamic bearing final design.

3 Simulation results and discussion

3.1 Turbine stress analysis

The critical parts of a turbine are those in contact with the intake steam, based on the concept that the mechanical characteristics of a metal undergo major modifications with the increasing temperature [9, 19]. The parameters analyzed in the selection of possible materials for the turbine rotor-blade structural analysis by FEM were good corrosion and oxidation resistance, high creep resistance, low density, and high mechanical properties. Steel has been the most widely used material in turbine development, due to its high mechanical resistance, high corrosion resistance, and an inert material [19, 20]. However, they are composed of expensive alloying elements—chrome, molybdenum, nickel, vanadium, magnesium—besides high density (7870 kg m^{-3}). Because of this, it was chosen to compare the steel behavior with an aluminum alloy, because this material is three times lighter than steel [20]. Thus, the selected materials were the AISI 420 martensitic stainless steel, the SAE 4340 steel, and the 7075-T6 aluminum alloy, indicated for applications in structures under high stress (Table 4).

Table 4 Main properties of the materials under stress analysis

Property	AISI 420	SAE 4340	7075-T6
Density (kg m^{-3})	8000	7850	2810
Young's modulus (GPa)	195	210	75
Poisson's ratio	0.27	0.30	0.33
Shear modulus (GPa)	77	80	26.9
Tensile strength (MPa)	655	1980	570
Yield strength (MPa)	275	1800	505
Fracture strength (MPa)	1095	2250	2042

Initially, support restrictions were defined, in which there is a coupling on the surface of the turbine rotor socket, besides to the addition of contact restriction throughout the turbine full-arc outer surface—simulating the steam turbine housing. FEM mesh will create a model that contains volumes, areas, lines and key points, etc., solid model entities in addition to elements and nodes. The proper definition of boundary conditions is a critical point in FEM computational simulations due to the need to limit the domain of the model, producing an artificial contour close to the real. This effect was obtained by fixing on the rotor coupling region to the displacement and rotation restrictions, since that the resulting stress is directly proportional to the centrifugal force generated by the system rotational movement [9]. The closer to the real operating conditions the boundary constraints are applied, the more reliable the results are obtained. The option available for generating the 3D FEM mesh model is shown in Fig. 3. von Mises method was used in the stress and strain analyses of the structures, criterion that presents more reliable results since it considers as reference the intermediate stress [21, 22], acting in the elastic deformation region of the materials. The stress analysis for the given three materials has been carried out under an operating speed of 30,000 RPM and has kept constant throughout the analysis. SolidWorks Simulation software was used for FEM study of the turbine rotor, and the results are mentioned below.

Figure 4 shows the von Mises stress induced in the turbine rotor for AISI 420 stainless steel. The maximum stress founded was 1138 MPa—4.14× greater than its yield

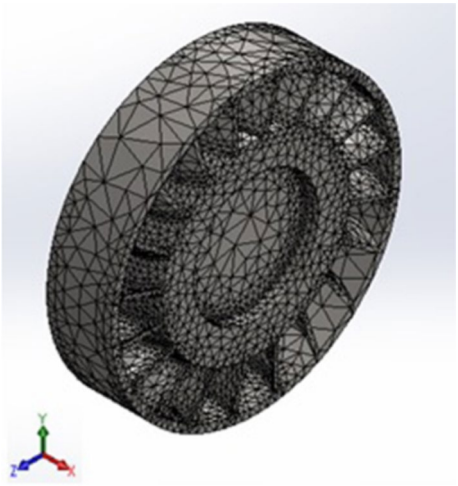

Fig. 3 Contour and 3D FEM mesh conditions used for stress analyses of the steam turbine rotor blade

strength. It is observed that the maximum stress (Fig. 4a), as well as the maximum strain (Fig. 4b), occurs in the regions close to the rotor coupling—aggravated by the rotor center mass displacement, and promoted by centrifugal force—and in the steam outlet region, since it is the largest area with pressure incidence. Factor of safety (FOS) is a term describing the structural capacity of a system beyond the applied loads or actual loads [19, 23]. A calculated ratio of structural capacity to actual applied load (Eq. 9) is as follows:

$$\mathrm{FOS} = \frac{\text{yield strength}}{\text{Von Mises stress}} \tag{9}$$

The FOS value must be a number greater than 1, in order to avoid greater possibility of component failure. In the present work, the FOS value was determined from 1.2, indicating that the turbine rotor blade can tolerate 20% greater effort than the load applied. Strain life approach is used to calculate the fatigue life of the turbine rotor according to Muralidharan and Manson equation (Eq. 10), where $\in_f$ is the fatigue ductility coefficient; S_u is the ultimate stress; $\Delta \in$ is the obtained strain; E is the Young's modulus; and N_f is the number of cycles [24].

$$\frac{\Delta \in}{2} = 0.623\left(\frac{S_u}{E}\right)^{0.832}\left(2N_f\right)^{-0.09} + 0.0196\left(\in_f\right)^{0.155}\left(\frac{S_u}{E}\right)^{-0.53}\left(2N_f\right)^{-0.56} \tag{10}$$

It can be observed that the maximum strain induced is equal to 0.3302 mm. In this way, the fatigue life cycles for AISI 420 martensitic stainless steel are limited at around 5.068e3. The results suggested that the component will rupture under the conditions presented, since the stress values obtained from FEM analyses exceed the material yield strength, indicating that it will not withstand the efforts required. Figure 5 presents the maximum von Mises stress and strain distribution in the turbine rotor for 7075 aluminum alloy. The component did not suffer any premature fractures. The maximum stress value founded was 399.6 Mpa (Fig. 5a)—20.8% less than its yield strength. In addition, the turbine rotor exhibited a maximum strain of 0.4584 mm (Fig. 5b), relatively low compared to the component movement accuracy, with a FOS = 1.264, and a fatigue life cycles at around 3.649e3. Although these values are practically at the stipulated limit, the results of 7075 aluminum alloy may be considered acceptable. Figure 6 exhibits the maximum von Mises stress and strain distribution in the turbine rotor for SAE 4340 steel. The maximum stress founded was 1089 MPa, and the maximum strain induced is equal to 0.2483 mm, with a FOS = 1.653, and the fatigue life cycles at around 8.659e3. The results obtained from the

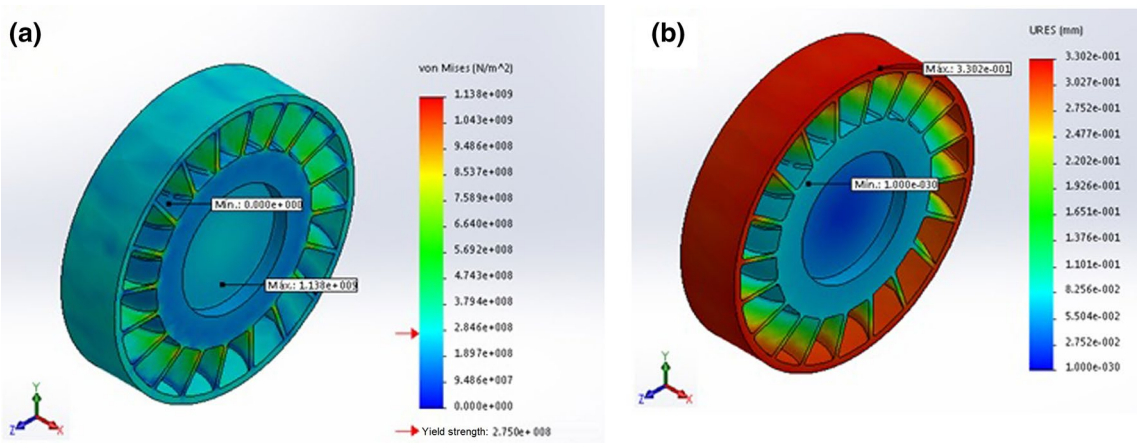

Fig. 4 **a** Maximum von Mises stress and **b** strain distribution of turbine rotor blade for AISI 420 martensitic stainless steel

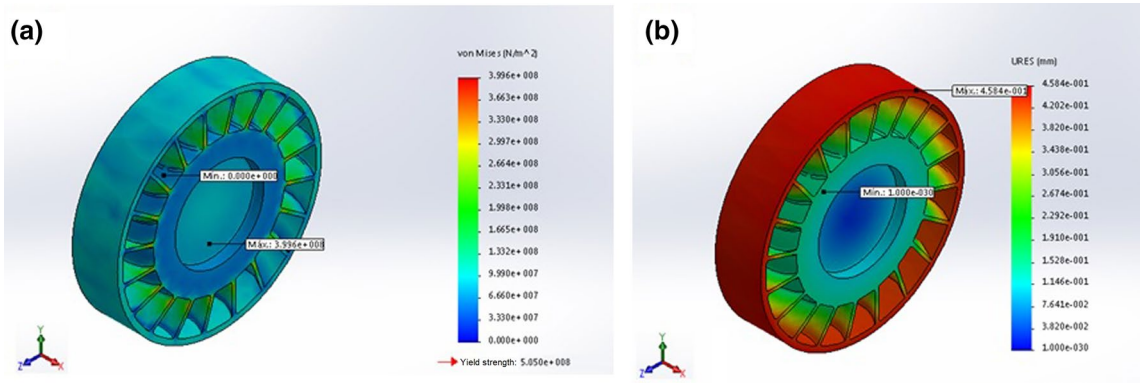

Fig. 5 **a** Maximum von Mises stress and **b** strain distribution of turbine rotor blade for 7075-T6 aluminum alloy

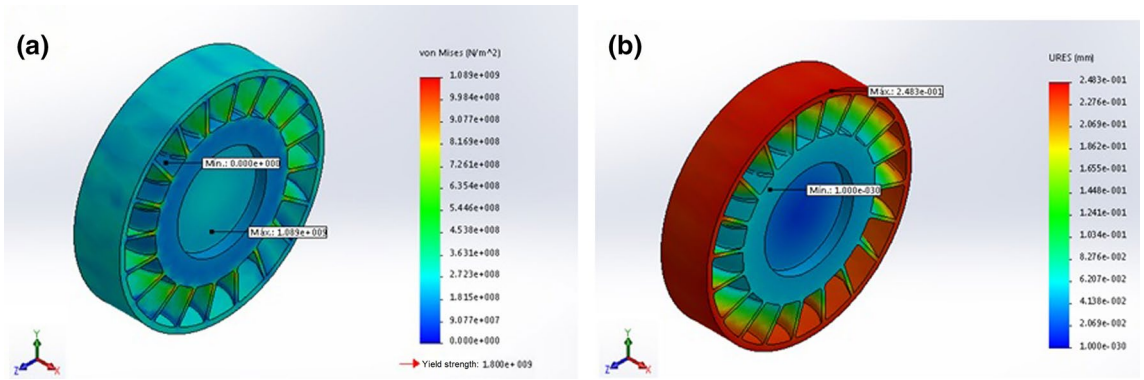

Fig. 6 **a** Maximum von Mises stress and **b** strain distribution of turbine rotor blade for SAE 4340 steel

Table 5 Summary of FEM simulation results for the three materials

	AISI 420	SAE 4340	7075-T6
Yield strength (MPa)	275	1800	505
Maximum stress (MPa)	1138	1089	399.6
Maximum strain	0.3302	0.2483	0.4584
Factor of safety	0.242	1.653	1.264
Fatigue life cycles	5.068e3	8.659e3	3.649e3

stress analysis are presented in Table 5, and also the FOS and fatigue life of the turbine rotor are calculated using strain life approach. Thus, for an operating speed of 30,000 RPM, the SAE 4340 steel presents as an excellent alternative for the de Laval steam turbine development, since the maximum von Mises stress endured by the turbine rotor blade was only 60.5% its yield strength, and the maximum strain was 55% smaller than the displacement that showed with the 7075-T6 aluminum alloy, with the highest FOS presented in all FEM simulations.

3.2 Hydrodynamic bearing stress analysis

Several materials have been commonly used in the manufacture of the hydrodynamic bushing bearings [9, 20], among which stand out the bronze alloys, aluminum alloys, sintered metals, nylon, and Teflon. The coefficient of linear thermal expansion φ is an important material property to define the bushing construction material. According to Eq. 11, D is the bushing diameter (mm) and d is the shaft diameter (mm). The result indicated that the leaded tin bronze alloy is the material with the most suitable characteristics.

$$\varphi = \frac{D - d}{d} \tag{11}$$

The presence of lead (Pb) is responsible for preventing or retarding the mechanical locking of the bushing/shaft assembly, prolonging the bearing fatigue life [25]. Specifically, the use of TM 23 and TM 620 bronze alloys was determined for the FEM analyses due to their chemical characteristics and mechanical properties (Table 6).

Inventor® Autodesk software was used for stress analysis of the bush hydrodynamic bearing under an operating speed of 30,000 RPM, a radial load of 93 N, a torque

Table 6 Comparison of chemical characteristics and mechanical properties of the TM 23 and TM 620 leaded tin bronze alloys

	Chemical characteristics				Mechanical properties					
	Copper (at.%)	Tin (at.%)	Zinc (at.%)	Lead (at.%)	Density (kg m^{-3})	Young's modulus (GPa)	Yield strength (MPa)	Fracture strength (MPa)	Hardness (HB 10)	Poisson's ratio
TM 23	73	4	8	15	9045	103	157	275	75	0.30
TM 620	87	8	4	1	8830	109	167	350	92	0.32

value of 15.915 N m, and a minimum centrifugal force of 23.8×10^3 N. The results obtained by the FE analysis suggested that the TM 23 bronze alloy did not suffer deformation or premature fracture under the conditions requested. The maximum von Mises stress value founded was 125 MPa, 20.4% less than its yield strength (Fig. 7a), with an excellent FOS = 2.2. Besides, the maximum strain induced in the bushing bearing over the simulation is equal to 0.007972 mm—relatively low in relation to the component movement accuracy and the stresses required by the system. Thus, it is noted that the TM 23 bronze alloy can be used for the bushing bearing development under these conditions. Figure 8 shows the static analysis results for the TM 620 bronze alloy. It is possible to observe that the respective material did not withstand the load required, since the maximum von Mises stress founded was, approximately, 233 MPa—around 39% above its yield strength. Although TM 23 bronze alloy has a lower mechanical strength than the TM 620 alloy, the same presents in its composition around 15% more lead—element that optimizes its self-lubricating properties [20, 25], which reduces its coefficient of friction and facilitates the bushing bearing rotational movements. In this way, the TM 620 bronze alloy is suitable for systems applications at low rotations.

4 Conclusions

The present research has shown a high-speed turbogenerator machine supported by hydrodynamic bearings to be used in biogas systems to generate electrical energy. To achieve this, a de Laval steam turbine rotor-blade model was designed using a methodology based on the mathematical control of characteristics. Finite element stress analysis was carried out for the moving turbine rotor blades, and for bush bearing, selecting the material which has better behavior under a constant operating speed of 30,000 RPM. Considering the pressures, forces, and restrictions applied on the high-speed turbogenerator assembly, after the structural analyses carried out by the finite element method, it was concluded that the maximum von Mises stress values obtained during the simulations are associated with the centrifugal force generated by the system rotational movement. Thus, taking into account that such action is directly proportional to the rotor radius length, and the angular velocity modulus, it is noted that the results variation was mainly due to the properties and chemical composition of the materials proposed in the study. For the steam turbine, AISI 420 stainless steel should not be used, because its low yield strength does not withstand the stresses caused by high speed of the turbine rotor. On the other hand, the 7075 aluminum alloy and the SAE 4340 steel obtained satisfactory results when

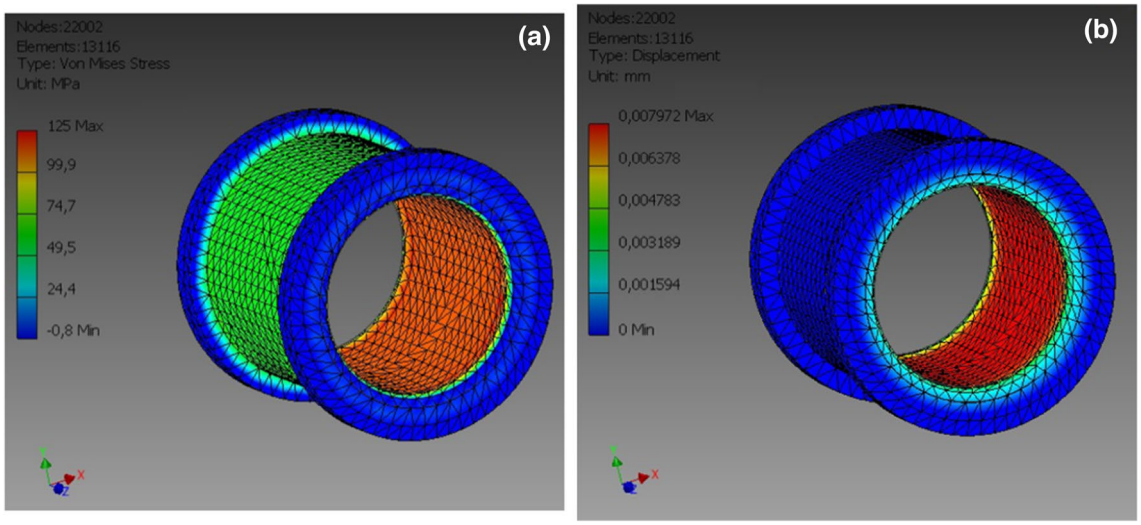

Fig. 7 **a** Maximum von Mises stress and **b** strain distribution of hydrodynamic bushing bearing for TM 23 leaded tin bronze alloy

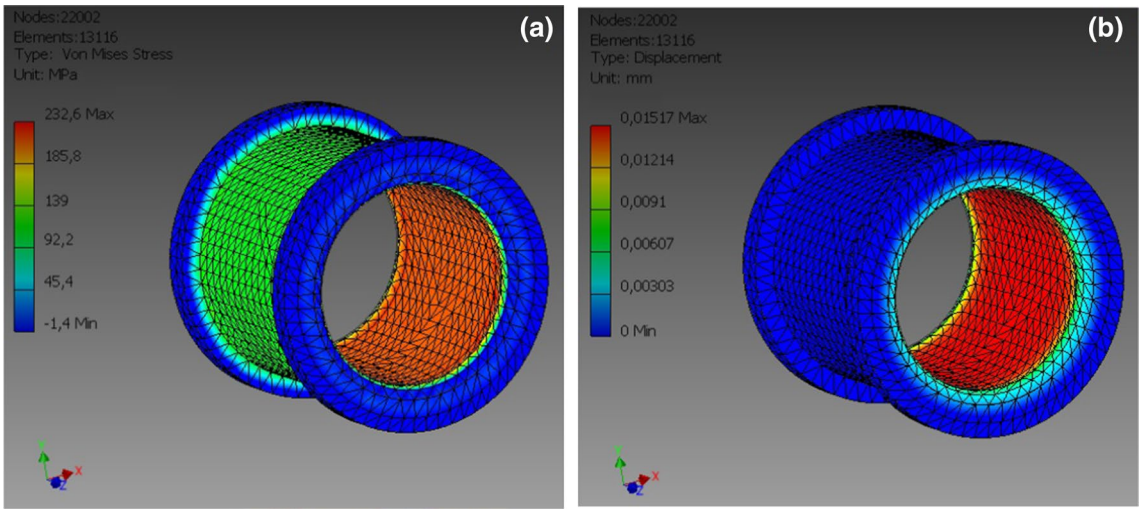

Fig. 8 **a** Maximum von Mises stress and **b** strain distribution of hydrodynamic bushing bearing for TM 620 leaded tin bronze alloy

subjected to efforts under the same conditions, particularly the SAE 4340 steel, since it was the material that presented the greatest factor of safety, in this way, being the indicated material for the turbine rotor-blade development. For the hydrodynamic bearing, the TM 23 bronze alloy exhibited excellent results, which makes evident its use for the development of the respective component. The TM 23 bronze alloy withstood the efforts that were required during the FEM simulation, without fracture, and presenting low mechanical deformation. Future improvement may include analysis of the vibration phenomena in the blades, EHL and tribological experiments, a full fluid–structure interaction model, and FE simulations of the first elastic vibration mode for the shaft.

Compliance with ethical standards

Conflict of interest The authors declare no conflict of interest.

References

1. Hamann T (2014) Perovskites take lead in solar hydrogen race. Science 345:1566–1567. https://doi.org/10.1126/science.1260051
2. Lamas W, Giacaglia G (2013) The Brazilian energy matrix: evolution analysis and its impact on farming. Energy Policy 63:321. https://doi.org/10.1016/j.enpol.2013.09.009

3. Lima LP, Ribeiro GBD, Perez R (2018) The energy mix and energy efficiency analysis for Brazilian dairy industry. J Clean Prod 181:209–216. https://doi.org/10.1016/j.jclepro.2018.01.221
4. Maia TAC, Faria OA, Barros JEM, Porto MP, Cardoso Filho BJ (2017) Test and simulation of an electric generator driven by a micro-turbine. Electr Power Syst Res 147:224–232. https://doi.org/10.1016/j.epsr.2017.02.033
5. Rosa FC, Lima F, Fumagalli MA (2017) A high-speed shaft supported by magnetic bearings applied to energy systems. J Braz Soc Mech Sci Eng 39:29–39. https://doi.org/10.1007/s40430-016-0650-3
6. Paniagua G, Iorio MC, Vinha N, Sousa J (2014) Design and analysis of pioneering high supersonic axial turbines. Int J Mech Sci 89:65–77. https://doi.org/10.1016/j.ijmecsci.2014.08.014
7. Machado TH, Cavalca KL (2015) Modeling of hydrodynamic bearing wear in rotor-bearing systems. Mech Res Commun 69:15–23. https://doi.org/10.1016/j.mechrescom.2015.05.008
8. Zhay L, Liu X, Chen F, Xiao Y, Wang Z (2014) Numerical simulations for the fluid-thermal-structural interaction lubrication in a tilting pad thrust bearing. Eng Comput 34:1149–1165. https://doi.org/10.1108/EC-08-2015-0209
9. Melconian S (2011) Elementos de máquinas. Érica, São Paulo
10. Chasalevris AC, Nikolakopoulos PG, Papadopoulos CA (2013) Dynamic effect of bearing wear on rotor-bearing system response. J Vib Acoust 135:011008. https://doi.org/10.1115/1.4007264
11. Zhay L, Luo Y, Wang Z, Liu X (2016) 3D two-way coupled TEHD analysis on the lubricating characteristics of thrust bearings in pump-turbines by combining CFD and FEA. Chin J Mech Eng 29:112–123. https://doi.org/10.3901/CJME.2015.0922.113
12. Usman A, Park CW (2018) Numerical optimization of surface texture for improved tribological performance of journal bearing at varying operating conditions. Ind Lubr Tribol 70:1608–1618. https://doi.org/10.1108/ILT-10-2017-0286
13. Nguyen VD, Jansson J, Goude A, Hoffman J (2019) Direct finite element simulation of the turbulent flow past a vertical axis wind turbine. Renew Energy 135:238–247. https://doi.org/10.1016/j.renene.2018.11.098
14. Komori M, Hara K, Asami K, Sakai N (2018) Trial of superconducting magnetic bearings applied to high-speed turbine rotor. IEEE Trans Magn 54:1–4. https://doi.org/10.1109/TMAG.2018.2841993
15. Rezaei MM, Zohoor H, Haddadpour H (2018) Aeroelastic modeling and dynamic analysis of a wind turbine rotor by considering geometric nonlinearities. J Sound Vib 432:653–679. https://doi.org/10.1016/j.jsv.2018.06.063
16. Yao J, Liu L, Yang F, Scarpa F, Gao J (2018) Identification and optimization of unbalance parameters in rotor-bearing systems. J Sound Vib 431:54–69. https://doi.org/10.1016/j.jsv.2018.05.050
17. Arakawa K (2014) Effect of time derivative of contact area on dynamic friction. Appl Phys Lett 104:241603. https://doi.org/10.1063/1.4884055
18. Kiehl M (2001) Einführung in die DIN-Normen. Springer, Berlin. https://doi.org/10.1007/978-3-322-92719-4
19. Askeland DR, Fulay PP, Wright WJ (2010) The science and engineering of materials. CENGAGE Learning, São Paulo
20. Callister WD Jr, Rethwisch DG (2009) Material science and engineering: an introduction. Wiley, New York
21. Ji DM, Sun JQ, Dui Y, Ren JX (2017) The optimization of the start-up scheduling for a 320 MW steam turbine. Energy 125:345–355. https://doi.org/10.1016/j.energy.2017.02.139
22. Li H, Li J, Yuan H (2018) A review of the extended finite element method on macrocrack and microcrack growth simulations. Theor Appl Fract Mech 97:236–249. https://doi.org/10.1016/j.tafmec.2018.08.008
23. Kumar D, Sarkar S (2016) Numerical investigation of hydraulic load and stress induced in Savonius hydrokinetic turbine with the effects of augmentation techniques through fluid-structure interaction analysis. Energy 116:609–618. https://doi.org/10.1016/j.energy.2016.10.012
24. Madhu P (2016) Stress analysis and life estimation of gas turbine blisk for different materials of a jet engine. Int J Sci Res 5:1103–1107. https://doi.org/10.21275/v5i6.NOV164440
25. Termomecanica São Paulo S.A, Bronze alloys catalogue. https://www.termomecanica.com.br/download/conteudo_tecnico/bronze.pdf. Accessed 9 Nov 2018